https://doi.org/10.30799/jnst.293.20060201 J. Nanosci. Tech. - Volume 6 Issue 2 (2020) 882–885

Share Your Innovations through JACS Directory

Journal of Nanoscience and Technology

Visit Journal at http://www.jacsdirectory.com/jnst

ISSN: 2455-0191

Conductivity and Dielectric Studies on Combustion Derived Self-Doped Ceria Nanoparticles

M.V. Hemantha Reddy[1,2], T. Sreenivasulu Reddy[1], R. Hari Krishna[3,*], M.N. Chandraprabha[4], M. Sasikumar[5]

[1]*Department of Physics, Dr. Ambedkar Institue of Technology, Bangalore – 560 056, Karnataka, India.*
[2]*Visveswaraya Technological University, Belagavi – 590 018, Karnataka, India.*
[3]*Department of Chemistry, M. S. Ramaiah Institute of Technology, Bangalore – 560 054, Karnataka, India.*
[4]*Department of Biotechnology, M. S. Ramaiah Institute of Technology, Bangalore – 560 054, Karnataka India.*
[5]*PG and Research Department of Physics, Bishop Heber College, Tiruchirappalli – 620 017, Tamil Nadu, India.*

ARTICLEDETAILS

Article history:
Received 20 January 2020
Accepted 15 March 2020
Available online 02 May 2020

Keywords:
Combustion Synthesis
Self-Doped CeO_2
AC Conductivity

ABSTRACT

A series of Ce^{4+} (0-25 mol%) doped ceria nanoparticles were prepared by low temperature combustion process using the fuel oxalyldihydrazide (ODH). Crystallographic information, formation of phase and micro structural details of prepared samples was obtained by using powder X-ray diffraction (PXRD) technique, Fourier transmission infrared (FTIR) spectroscope and field emission scanning electron microscope (FESEM) technique respectively. The size (10–30 nm) of self-doped ceria nanoparticles are evaluated by transmission electron microscope (TEM). PXRD studies confirm the fluorite structure of nanoceria with JCPDS card No. 034-0394. Conductivity and dielectric studies for self-doped ceria nanoparticles were performed in the applied frequency from 20 Hz to10 MHz and at different temperatures (200-560 °C). The temperature and frequency dependence of the conductivity and dielectric properties of prepared samples showed major effect of the dopant concentration. Dielectric constant and tangent loss of prepared samples decreased sharply with increasing frequency.

1. Introduction

Rare earth oxides are being used as polishing compounds, phosphors, catalysts, etc., due to their good optical, electrical and chemical properties [1]. Cerium oxide has attracted the interest of many researchers due to its diverse applications in different areas like biomedical sciences, materials sciences etc., [2-6]. Compared to un-doped nanoceria, rare earth doped nanoceria was found to be true electrolyte material for the application of solid oxide fuel cells in moderate temperature 500-700 °C contrast to conventional yttria-stabilized zirconia [7]. The impurities like aliovalent-dopants [8-12] addition drastically increase the ionic conductivity of un-doped ceria due to the creation of oxygen vacancies that indirectly help the migration of ions. In doped ceria, oxygen ion conductivity takes place on basis of hopping mechanism [13] and has a direct bearing on the type and ratio of dopant ion concentration of and also on the oxygen vacancies and defect structure. The major problem in solid electrolyte materials is the increase of conductivity due to electrons, high operating temperature reduces the valence state of Ce^{4+} to Ce^{3+} [14] and segregation/splitting-up of impurities at grain boundaries [15,16] leading to poor long-term stability. The correlation between dielectric behaviour and ionic conductivity for perovskite dielectric systems such as multiferroics, ferroelectrics and antiferroelectrics has been well studied [17-19]. In the present work, structural, morphology and AC conductivity and dielectric studies were investigated for Ce^{4+} (0-25 mol%) doped ceria nanopowder. Low temperature densification of nanoceria materials has been achieved by employing wet chemical synthesis methods [21,22]. Among the various wet chemical preparation methods, solution combustion synthesis (SCS) technique is considered to be a relatively better technique due to low cost, fast reaction time (within 5 minutes) and simple experimental setup [23-25]. In the present study, SCS technique has been employed to synthesize the samples.

2. Experimental Methods

2.1 Synthesis

Combustion method is applied to synthesize CeO_2:Ce^{4+} (0-25 mol%) nanopowder using laboratory prepared oxalyldihydrazide (ODH) as fuel. Stoichiometric quantities of cerium nitrate ($Ce(NO_3)_3{\cdot}6H_2O$) and ODH ($C_2H_6N_4O_2$) were added into a beaker containing 35 mL of double distilled water and then the solution was blended for about 5 min to obtain a homogeneous solution. The solution containing beaker was kept in a preheated high temperature furnace maintained at 400 ± 10 °C to initiate the combustion process and to obtain the nano powder sample.

2.2 Characterization

PXRD patterns of all the sample are obtained using Powder X-ray diffract-meter [Bruker AXS D8 and Cu K_α- 1.5418 Å] in 20°-80° diffraction angle (2θ) range. The Fourier transform infrared (FT-IR) spectra of prepared samples were examined at room temperature using IR Affinity-1 (Shimadzu, Japan) spectrometer. The micro-structural information of the samples was obtained by examining them using FESEM instrument (Tescan-Mira 3 LMH, magnification: 2X to 10,00,000X, accelerating voltage: 50 V to 30 kV in steps of 10 V). High resolution transmission electron microscope (HR-TEM) images of the nanopowder were analysed (Jeol /JEM-2100, accelerating voltage up to 200 kV) to determine particle size. Debye - Scherrer formula was used to determine crystallite size of nanopowder. The calcined samples were subjected to a uniaxial pressure of 6.5 tons/m^2 to obtain pellets. Mechanical Strength of the pellets is increased by sintering them at 600 °C for 2 hours. The above and below surfaces of the circular pellets were uniformly coated with conducting material like silver paste. The AC conductivity and dielectric behaviour of the samples were studied at different temperatures (200 -560 °C) and at different frequencies (20 Hz – 10 MHz) using precision impedance analyzer (Model 6515B-15MHz series, Wayne Kerr electronics).

3. Result and Discussion

Fig. 1 represents the PXRD patterns of un-doped and CeO_2:Ce^{4+} (0 – 25 mol%) nanoparticles, the sharp intense peaks related to the miller indices (111), (2 0 0), (2 2 0), (3 1 1), (2 2 2), (4 0 0) and (3 3 1) confirming the cubic fluorite structure of the samples [JCPDS card No. 034-0394]. Debye

*Corresponding Author:rhk.chem@gmail.com(R. Hari Krishna)

https://doi.org/10.30799/jnst.293.20060201

Cite this Article as: M.V. Hemantha Reddy, T. Sreenivasulu Reddy, R. Hari Krishna, M.N. Chandraprabha, M. Sasikumar, Conductivity and dielectric studies on combustion derived self-doped ceria nanoparticles, J. Nanosci. Tech. 6(2) (2020) 882–885.

Scherrer's formula was employed to determine crystallite size 'D' (10-20 nm) [26] of the samples,

$$D = \frac{K\lambda}{\beta\cos\theta} \quad (1)$$

where, K, λ, X, and β represents shape factor (spherical structure), wavelength of rays and band width of diffraction peak.

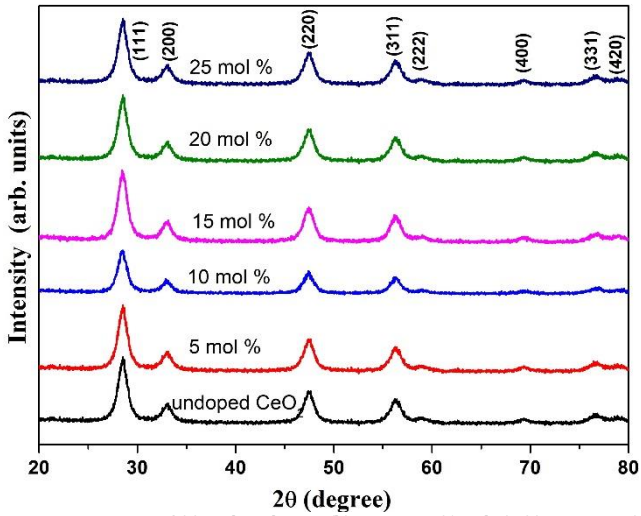

Fig. 1 PXRD patterns of (a) undoped CeO_2, (b) CeO_2:Ce^{4+} (5 mol%), (c) CeO_2:Ce^{4+} (10 mol%), (d) CeO_2:Ce^{4+} (15 mol%), (e) CeO_2:Ce^{4+} (20 mol%), (f) CeO_2:Ce^{4+} (25 mol%)

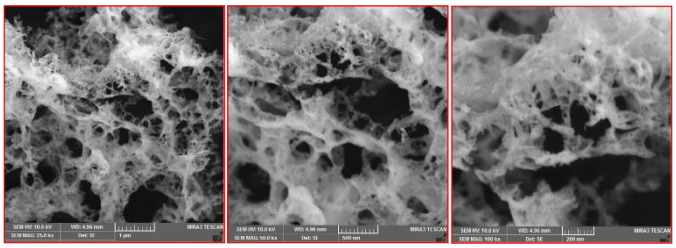

Fig. 2 SEM pictures of CeO_2:Ce^{4+} (15 mol%)

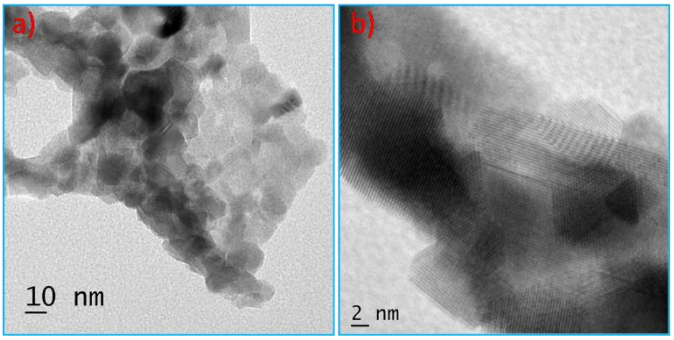

Fig. 3 (a) TEM and (b) HRTEM images of CeO_2:Ce^{4+} (15 mol%) nanoparticles

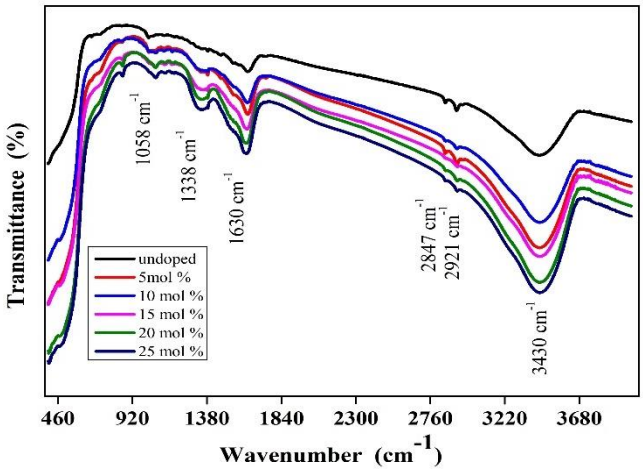

Fig. 4 FTIR graphs of (a) undoped CeO_2, (b) CeO_2:Ce^{4+} (5 mol%), (c) CeO_2:Ce^{4+} (10 mol%), (d) CeO_2:Ce^{4+} (15 mol%), (e) CeO_2:Ce^{4+} (20 mol%), (f) CeO_2:Ce^{4+} (25 mol%)

FESEM images of pure and Ce^{4+} doped ceria nanoparticles depicted in Fig. 2 indicate the presence of large number of voids and agglomerates. This implies a spongy and porous morphology of both the samples, thereby indicating insignificant influence of dopant ions on morphology. During the combustion process large quantities of gases get expelled leading to the formation of voids and porous structures [27, 28]. TEM and HR-TEM images of CeO_2:Ce^{4+} (15 mol%) samples were showed in Fig. 3. Fig. 3a indicates agglomerated non-uniform sized and nearly spherical structures with average particle size in the 10-30 nm range. Polycrystalline nature of the samples was observed in the high resolution TEM image (Fig. 3b).

The FTIR spectra of undoped and CeO_2:Ce^{4+} (0 – 25 mol%) doped ceria shown in Fig. 4 exhibit characteristic absorption at 3430 cm^{-1}, 2921 cm^{-1} 2847 cm^{-1}, 1630 cm^{-1}, 1338 cm^{-1} and 1058 cm^{-1}. The absorption at various wave-numbers corresponds to the stretching vibration of the hydrogen bonded OH group (3430 cm^{-1}). CH_2 group (2921 and 2847 cm^{-1}) and COO^{-1} group (1630 cm^{-1}) respectively. Absorption at 1338 cm^{-1} and 1058 cm^{-1} correspond to the presence of O–N group [29] and nitrate ions [30] respectively. Finally, the absorptions at 854–484 cm^{-1} can be ascribed to the characteristic Ce–O vibration. The absence of adsorbed water and enhancement in the crystallinity of the sample can be ascribed to the decrease in the band intensity due to sintering [31].

The complex dielectric constant of a material consists of an imaginary (ε'') and a real part (ε').

$$\varepsilon = \varepsilon' - j\varepsilon'' \quad (2)$$

$$\varepsilon'' = \varepsilon' \tan\delta \quad (3)$$

$$\varepsilon' = \frac{Cd}{\varepsilon_0 A} \quad (4)$$

where C, d, A, ε_0 and tan δ represent capacitance, thickness, area of the sample, permittivity of free space, and dielectric loss respectively. Fig. 5 represents the frequency- dielectric constant plot of CeO_2:Ce^{4+} (15 mol%) studied at various temperatures (200-560 °C). It can be inferred from the plot that the real part of dielectric permittivity (ε') shows a sharp upturn at the lower frequency regime and decreases exponentially with rise in applied frequency and relatively constant at higher frequencies regime. The exponential decay of real part (ε') can be ascribed to reduction of interfacial polarization effect. At low frequency regime the high value of ε' is attributed to the existence of polarization of charge carriers (oxygen ions) near the grain boundaries and the consequent creation of a potential barrier. The observed variation of ε' with frequency is in agreement with Maxwell-Wagner and Koop's theory [32, 33]. The increase of real part (ε') with rise in temperature can be ascribed to the swift orientation of electric dipoles [34, 35].

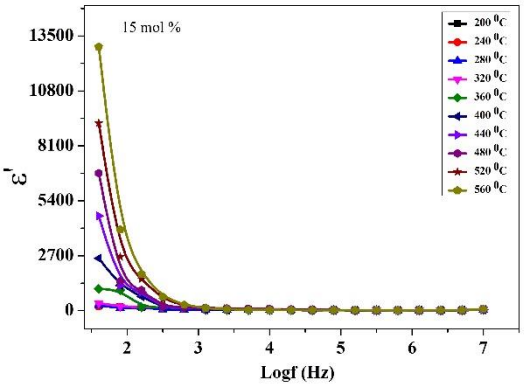

Fig. 5 The variation of relative dielectric constant with the applied frequency in the temperature range 200 °C -560 °C of 15 mol% Ce^{4+} doped CeO_2 nanoparticles

Fig. 6 represents the frequency-dielectric constant plots of all the samples at a particular temperature. It can be observed from the Fig. 6 that ε' rises with increase in dopant concentration and becomes maximum for a particular dopant concentration (15 mol%) and thereafter it decreases. This can be ascribed to reduction of defects concentration at higher dopant concentration. Fig. 7 shows that tangent loss (tan δ) versus frequency graph of 15 mol% Ce^{4+} doped ceria nanoparticles at various temperatures (200-560 °C). The variation between tan δ and frequency graph shows same trend exhibited by ε'. This behaviour is mainly due to the interfacial polarization of dipoles at the interface between the electrode and electrolyte. The presence of relaxation peak at higher temperatures and at a particular frequency can be ascribed to the dipole moment of defect pairs. The decrease of tan δ at higher frequencies may be ascribed to the phase lag between the orientation of the dipoles with the applied frequency [36, 37].

https://doi.org/10.30799/jnst.293.20060201

Cite this Article as: M.V. Hemantha Reddy, T. Sreenivasulu Reddy, R. Hari Krishna, M.N. Chandraprabha, M. Sasikumar, Conductivity and dielectric studies on combustion derived self-doped ceria nanoparticles, J. Nanosci. Tech. 6(2) (2020) 882–885,

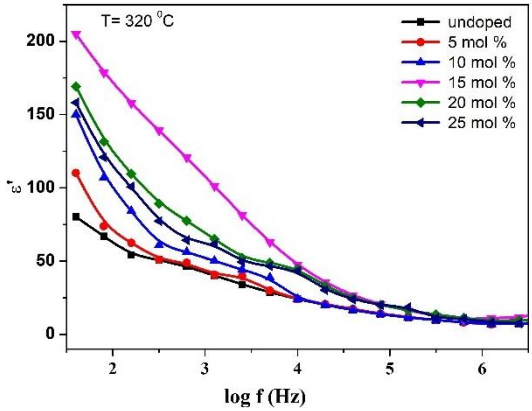

Fig. 6 Variation of dielectric constant as a function of dopant concentration of CeO_2:Ce^{4+} (0-25 mol%) nanoparticles

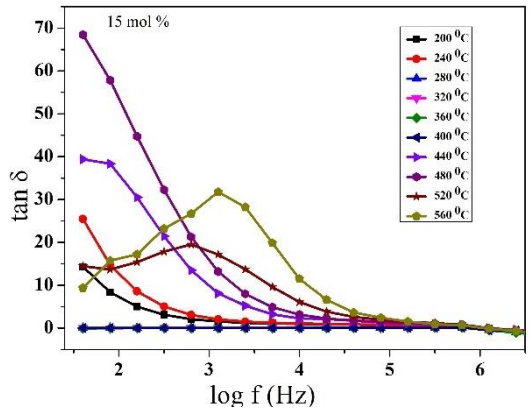

Fig. 7 Dielectric loss spectra of 15 mol% Ce^{4+} doped CeO_2 nanoparticles

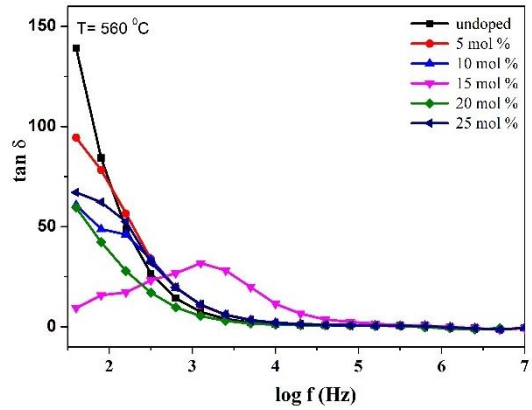

Fig. 8 variation of tan δ with applied frequency of undoped and CeO_2:Ce^{4+} (0 – 25 mol%) doped ceria nanoparticles

Fig. 8 represents the graph plotted between the tan δ and applied frequency of un-doped and Ce^{4+} (0 – 25 mol%) doped ceria nanoparticles at a particular temperature. The behaviour of high dielectric loss at low frequency regime is due to the interfacial polarization phenomena. Low dielectric loss and a relaxation peak observed for 15 mol% Ce^{4+} doped ceria nanoparticle can be ascribed to the dipole moment of oxygen vacancy- dopant ion dipoles.

AC conductivity of the Ce^{4+}:CeO_2 (0-25 mol%) samples were calculated using the basic formula,

$$\sigma = G \times \frac{d}{A} \quad (5)$$

where 'A' is the area of the pellet, 'd' is the thickness of the pellet and G represent the conductance of the sample. The frequency dependent conductivity studies of self-doped ceria samples at different temperatures are studied (figures not shown). The AC conductivity of Ce^{4+}:CeO_2 (0-25 mol%) is observed to be constant in the lower frequency regime and in the high frequency regime was found increase linearly as per the Jonscher's power law,

$$\sigma_w = \sigma_0 + A W^S \quad (6)$$

where σ_w represent AC conductivity, σ_0 represent limiting zero frequency conductivity, A represent pre-exponential constant, W represent angular frequency and s represent frequency exponent where 0 < s < 1 [38]. Hence, the AC conductivity at different temperatures (200-560 °C) in all the synthesized samples follows the universal power law [39].

Fig. 9 shows the graph plotted between conductivity and applied frequency at different self-dopant concentrations for a particular temperature. The observed conductivity behaviour of the all prepared samples can be described with the help of Jump Relaxation Model [40]. It can be observed from the figures that the conductivity is maximum for 15 mol percent self-doped ceria. This can be understood in the light of the inverse relation between the dielectric constant and the columbic force between oxygen vacancy and dopant ion,

$$F = \frac{-2e^2}{4\pi\varepsilon_0\varepsilon_r r^2} \quad (7)$$

where r- inter-ionic separation and ε_r -dielectric constant of material. It is pertinent to recall here that the variation of dielectric constant and AC conductivity with dopant concentration and temperature is identical. Hence higher the dielectric constant lower is the columbic interaction and higher is the AC conductivity of the material. The fall in conductivity was observed for 20 mol and 25 mol percent dopant concentration samples can be attributed to lower defects concentration. At higher dopant concentrations, Ce^{4+} ions compensate for the produced defects because similar ionic radius of dopant ion with host ion.

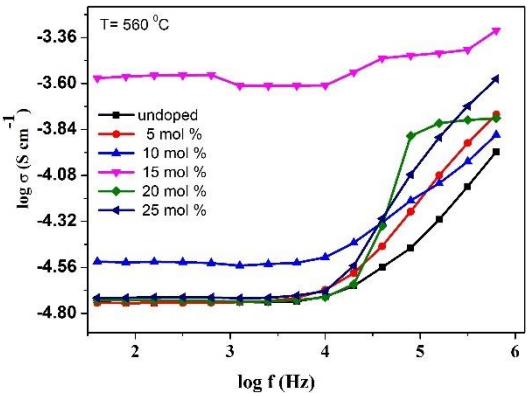

Fig. 9 Variation of conductivity as a function of frequency of 15 mol% Ce^{4+} doped CeO_2 nanoparticles

4. Conclusion

Ce^{4+} doped ceria nanopowder was synthesized using solution combustion route. PXRD studies reveal cubic fluorite structure of the material. Large voids and porous nature of the samples is confirmed by electron microscopy studies. Temperature, dopant concentration dependence of dielectric constant and conductivity on frequency of Ce^{4+} doped CeO_2 nanoparticles can be explained on the basis of hopping mechanism of the ions. The relatively higher conductivity observed for 15 mol % self-doped ceria sample can be understood in the light of the inverse relationship between the dielectric constant and columbic interaction force that binds the oxygen vacancy to the dopant ion.

Acknowledgement

We would like to acknowledge the Management and Principal of Dr. Ambedkar Institute of Technology for their assistance in procuring the impedance analyzer under TEQIP-II fund.

References

[1] D. Xue, K. Betzler, H. Hesse, Dielectric constants of binary rare earth compounds, J. Phys. Condens. Matter 12 (2000) 3113–3118.
[2] A.A. Ansari, J. Labis, M. Alam, S.M. Ramay, N. Ahmad, A. Mahmood, Influence of copper ion doping on structural, optical and redox properties of CeO_2 nanoparticles, J. Electroceram. 36 (2016) 150–157.
[3] J. Chen, S. Pati, S. Seal, J.F. McGinnis, Rare earth nanoparticles prevent retinal degeneration induced by intracellular peroxides, Nat. Nanotechnol. 1 (2006) 142–150.
[4] J. Colon, L. Herrera, J. Smith, S. Patil, C. Komanski, et al., Protection from radiation induced pneumonitis using cerium oxide nanoparticles, Nanomed. Nanotechnol. Biol. Med. 5 (2009) 225–231.
[5] A.A. Ansari, P.R. Solanki, B.D. Malhotra, Hydrogen peroxide sensor based on horseradish peroxidase immobilized nanostructured cerium oxide film, J. Biotechnol. 142 (2009) 179–184.

https://doi.org/10.30799/jnst.293.20060201

Cite this Article as: M.V. Hemantha Reddy, T. Sreenivasulu Reddy, R. Hari Krishna, M.N. Chandraprabha, M. Sasikumar, Conductivity and dielectric studies on combustion derived self-doped ceria nanoparticles, J. Nanosci. Tech. 6(2) (2020) 882–885,

[6] M.V. Hemantha Reddy, T. Sreenivasulu Reddy, R. Hari Krishna, B.M. Nagabhushana, M.N. Chandraprabha, Synthesis of Sm^{3+} doped nano ceria with compositionally tuneable conductivity and dielectric properties, Mater. Res. Express 6 (2019) 035023:1-35.
[7] B.C.H. Steele, A. Heinzel, Materials for fuel-cell technologies, Nature 414 (2001) 345-352.
[8] H. Arai, T. Kunisaki, Y. Shimizu, T. Seiyama, Electrical properties of calcia-doped ceria with oxygen ion conduction, Solid State Ionics 20 (1986) 241-248.
[9] K.C. Anjaneya, G.P. Nayaka, J. Manjanna, G. Govindaraj, K.N. Ganesha, reparation and characterization of $Ce_{1-x}Gd_xO_{2-\delta}$ (x = 0.1–0.3) as solid electrolyte for intermediate temperature, SOFC J. Alloys Compd. 578 (2013) 53-59.
[10] N. Jaiswal, D. Kumar, S. Upadhyay, O. Prakash, Ionic conductivity investigation in lanthanum (La) and strontium (Sr) co-doped ceria system, J. Power Sources 222 (2013) 230-236.
[11] S.J. Hong, K. Mehta, A.V. Virkar, Effect of microstructure and composition on ionic conductivity of rare-earth oxide-doped ceria, J. Electrochem. Soc. 145 (1998) 638-647.
[12] M. Dudek, Ceramic oxide electrolytes based on CeO_2—Preparation, properties and possibility of application to electrochemical devices, J. European Ceram. Soc. 28 (2008) 965-971.
[13] Raghvendra, R.K. Singh, P. Singh, Electrical conductivity of LSGM-YSZ composite materials synthesized via coprecipitation route, J. Mater. Sci. 49 (2014) 5571–5578.
[14] A.K. Baral, V. Sankaranarayanan, Ionic transport properties in nanocrystalline $Ce_{0.8}A_{0.2}O_{2-\delta}$ (with A = Eu, Gd, Dy, and Ho) materials, Nanoscale Res. Lett. 5 (2010) 637-643.
[15] M. Mogensen, N.M. Sammes, G. Tompsett, Physical, chemical and electrochemical properties of pure and doped ceria, Solid State Ionics 129 (2000) 63-94.
[16] R. Gerhardt, A.S. Nowick, Grain boundary effect in ceria doped with trivalent cations: I, electrical measurements, J. Am. Ceram. Soc. 69 (1986) 641-646.
[17] M.O. Zacate, L. Minervini, D.J. Bradfield, R.W. Grimes, K.E. Sickafus, Defect cluster formation in M_2O_3-doped cubic ZrO_2, Solid State Ionics 128 (2000) 243-254.
[18] A. Behera, N.K. Mohanty, B. Behera, P. Nayak, Impedance properties of 0.7 ($BiFeO_3$)-0.3 ($PbTiO_3$) composite, Adv. Mat. Lett. 4 (2013) 141-145.
[19] C.K. Suman, K. Prasad, R.N.P. Choudhary, Complex impedance studies on tungsten-bronze electroceramic: $Pb_2Bi_3LaTi_5O_{18}$, J. Mat. Sci. 41 (2006) 369-375.
[20] B.N. Parida, P.R. Das, R. Padhee, R.N.P. Choudhary, Synthesis and chracterization of a tungsten bronze ferroeletcric oxide, Adv. Mat. Lett. 3(3) (2012) 231-238.
[21] J.G. Li, T. Ikegami, J.H. Lee, T. Mori, Characterization and sintering of nanocrystalline CeO_2 powders synthesized by a mimic alkoxide method, Acta Mater. 49 (2001) 419-426.
[22] L.M.R. Jennifer, Tanja Drobek, Antonella Rossi, Ludwig J. Gauckler, Chemical analysis of spray pyrolysis gadolinia-doped ceria electrolyte thin films for solid oxide fuel cells, Chem. Mater. 19 (2007) 1134–1142.
[23] C. Kleinlogel, I.J. Gauckler, Sintering of nanocrystalline CeO_2 ceramics, Adv. Mater. 13 (2001) 1078-1081.
[24] S. Ekambaram, K.C. Patil, Combustion synthesis of yttria, J. Mater. Chem. 5 (1995) 905-908.
[25] S. Manjunatha, R. Hari Krishna, Tiju Thomas, B.S. Panigrahi, M.S. Dharmaprakash, Moss-Burstein effect in stable, cubic ZrO_2:Eu^{+3} nanophosphors derived from rapid microwave-assisted solution-combustion technique, Mater. Res. Bull. 98 (2018) 139-147.
[26] H.C Madhusudhana, S.N. Shobhadevi, B.M. Nagabhushana, B.V. Cheluvaraju, M.V. Murgendrappa, Effect of fuels on conductivity, dielectric and humidity sensing properties of ZrO_2 nanocrystals prepared by low temperature solution combustion method, J. Asian Ceram. Soc. 4 (2016) 309-3018.
[27] Bincy Rose Vergis, R. Hari Krishna, Nagaraju Kottam, B.M. Nagabhushana, R. Sharath, B. Darukaprasad, Removal of malachite green from aqueous solution by magnetic $CuFe_2O_4$ nano-adsorbent synthesized by one pot solution combustion method, J. Nanostruct. Chem. 8 (2018) 1-12.
[28] G. Ram Gopal, G. Krishna Reddy, R. Hari Krishna, A. Jagannatha Reddy, D.L. Monika, et al., Facile self-propagating combustion synthesis of MgO:Eu^{3+} orange-red nanophosphor and luminescence investigation by Judd-Ofelt intensity parameters, Optik174 (2018) 234-243.
[29] K.M. Girish, S.C. Prashantha, Ramachandra Naik, H. Nagabhushana, H.P. Nagaswarupa, et al., Visible photon excited photoluminescence; photometric characteristics of a green light emitting Zn_2TiO_4: Tb^{3+} nanophosphor for WLEDs, Mater. Res. Expr. 3 (2016) 075015:1-15.
[30] S. Shrestha, C.M.Y. Yeung, C. Nunnerley, S.C. Tsang, Comparison of morphology and electrical conductivity of various thin films containing nano-crystalline praseodymium oxide particles, Sens. Actuators A 136 (2007) 191–198.
[31] J. Tartaj, V. Gil, A. Moure, Low-temperature preparation by polymeric complex solution synthesis of Cu–Gd-doped ceria cermets for solid oxide fuel cells anodes: Sinterability, microstructures and electrical properties, J. Power Sources 195 (2010) 2800–2805.
[32] N. Shehata, K. Meehan, M. Hudit, N. Jain, Control of oxygen vacancies and Ce^{+3} concentrations in doped ceria nanoparticles via the selection of lanthanide element, J. Nanopart. Res. 14 (2012) 1173–1183.
[33] C.G. Koops, On the dispersion of resistivity and dielectric constant of some semiconductors at audio frequencies, Phys. Rev. 83 (1951) 121-124.
[34] Y.S. Asar, T. Asar, S. Altındal, S. Özçelik, Investigation of dielectric relaxation and ac electrical conductivity using impedance spectroscopy method in (AuZn)/TiO_2/p-GaAs (1 1 0) Schottky barrier diodes, J. Alloys Comp. 628 (2015) 442-449.
[35] A. Awadhia, S.K. Patel, S.L. Agarwal, Dielectric investigations in PVA based gel electrolytes, Prog. Cryst. Growth Charact. Mater. 52 (2006) 61-68.
[36] A.K. Yashar, Impedance spectroscopy (IS) and thermally stimulated discharged current (TSDC) studies on CdSe-PVA nanocomposites prepared by ultrasound-assisted method, Optoelect. Adv. Mater. Rapid Commun. 4 (2010) 174-179.
[37] J.P. Singh, S. Gautam, P. Kumar, A. Tripathi, J.M. Chen, et al., Correlation between the dielectric properties and local electronic structure of copper doped calcium titanate, J. Alloys Comp. 572 (2013) 84-88.
[38] M.D. lngram, Ionic conductivity in glass, Phys. Chem. Glass. 28 (1987) 215-234.
[39] Ashok Kumar Baral, V. Sankaranarayanan, Grain size effect on electrical and dielectric properties of the nanostructured Dy-doped ceria $Ce_{0.8}Dy_{0.2}O_2$, J. Electrochem. Soc. 157 (2010) P53-P58.
[40] H. Pazhani, P. Kumar, A. Varghese, A. Moses Ezhil Raj, S. Solomon, J. K.Thomas, Synthesis, vacuum sintering and dielectric characterization of zirconia (t-ZrO_2) nanopowder, J. Alloys Compd. 509 (2011) 6819–6823.

https://doi.org/10.30799/jnst.293.20060201

Cite this Article as: M.V. Hemantha Reddy, T. Sreenivasulu Reddy, R. Hari Krishna, M.N. Chandraprabha, M. Sasikumar, Conductivity and dielectric studies on combustion derived self-doped ceria nanoparticles, J. Nanosci. Tech. 6(2) (2020) 882–885,